ACS OMEGA

Open Access

http://pubs.acs.org/journal/acsodf

Article

Effects of Benzo (*a*) Pyrene and 2,2′,4,4′-Tetrabromodiphenyl Ether Exposure on the Thyroid Gland in Rats by Attenuated Total Reflection Fourier-Transform Infrared Spectroscopy

QiuFeng Lao,[⊥] LiJun Yang,[⊥] ShuZhen Liu, XiaoJun Ma, DeChan Tan, JinBo Li, BaoYi Liao, YuanFeng Wei, WeiYi Pang, Camilo L. M. Morais,* and Hui Liu*

Cite This: *ACS Omega* 2024, 9, 4317−4323

Read Online

ACCESS | Metrics & More | Article Recommendations

ABSTRACT: Benzo[*a*]pyrene (B[*a*]P) and 2,2′,4,4′-tetrabromodiphenyl ether (BDE-47) are widespread environmental pollutants and can destroy thyroid function. We assessed the biochemical changes in the thyroid tissue of rats exposed to B[*a*]P and BDE-47 using attenuated total reflection Fourier-transform infrared spectroscopy combined with support vector machine(SVM). After B[*a*]P and BDE-47 treatment in rats, the structure of thyroid follicles was destroyed and epithelial cells were necrotic, indicating that B[*a*]P and BDE-47 may lead to changes of the thyroid morphology of the rats. These damages are mainly related to C═O stretch vibrations of lipids (1743 cm^{-1}), as well as the secondary structure of proteins [amide I (1645 cm^{-1}) and amide II (1550 cm^{-1})], and carbohydrates [C−OH (1138 cm^{-1}), C−O (1106 cm^{-1}, 1049 cm^{-1}, 991 cm^{-1}), C−C (1106 cm^{-1}) stretching] and collagen (phosphodiester stretching at 922 cm^{-1}) vibration modes. When SVM was used for classification, there was a substantial separation between the control and the exposure groups (accuracy = 96%; sensitivity = 98%; specificity = 87%), and there was also a major separation between the exposed groups (accuracy = 93%; sensitivity = 94%; and specificity = 92%).

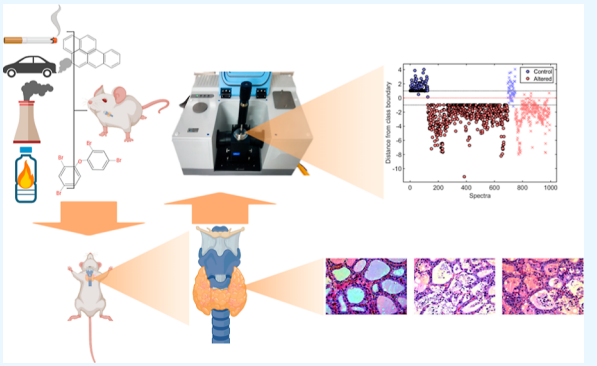

1. INTRODUCTION

Polycyclic aromatic hydrocarbon (PAHs) compounds are a common type of environmental pollutants, which are mainly formed by incomplete combustion of organic materials and widely distributed in the atmosphere and are identified as suspected carcinogens. PAHs entering the atmosphere can be transported over long distances and then deposited into vegetation, water bodies or soil by atmospheric precipitation.[1,2] PAHs may directly interfere with thyroid function and then change the thyroid structure, leading to the interruption of hormone synthesis, thus reducing thyroid hormone (TH) circulation and tissue level.[3] The most representative PAHs is B[*a*]P, which can be absorbed through the skin, respiratory, and digestive tract and has become a public health concern due to its carcinogenic, teratogenic, and mutagenic effects.[4,5]

Polybrominated diphenyl ethers (PBDEs) are widely used as brominated flame retardants in various consumer products such as plastics, rubber, textiles, furniture, and electronic equipment, but they can easily escape from products into the environment. People can be exposed to PBDEs through dust, air, and food; thus, PBDEs pose a threat to health.[6,7] 2,2′,4,4′-Tetrabromodiphenyl ether (BDE-47) is one of the most predominant PBDE congeners detected in the environment and human samples,[8] with the characteristics of lipophilicity, biological accumulation, degradation resistance, and toxicity. Since BDE-47 is structurally similar to triiodothyroxine (T3) and thyroxine (T4), it is thought to disrupt TH levels and related functions in adult and developing animals.[9−11] Other studies have shown that BDE-47 is negatively correlated with T3 and serum free thyroxine and positively correlated with thyrotropin, thereby affecting thyroid function.[12,13]

There are many analytical techniques available to monitor chemical pollutants in ecosystems and living organisms. Attenuated total reflection Fourier-transform infrared (ATR-FTIR) spectroscopy is an analytical technique that is nondestructive to the samples; relatively free of reagents; fast, being capable of producing results in real time; with high-throughput and reliability; and highly sensitive to small bimolecular changes.[14] Biomolecules exhibit responses to different wavelengths of light, and the resulting spectra can

Received: August 13, 2023
Revised: December 23, 2023
Accepted: January 4, 2024
Published: January 19, 2024

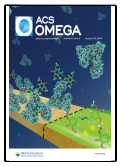

be considered as a "biochemical-cell fingerprint" (biofingerprint) of the sample. Cell or tissue types with underlying cellular features can be distinguished according to the changes in biological fingerprints.[14,15] Spectroscopy has increasingly been combined with machine learning and classification algorithms as tools to identify and distinguish disease states. Recent studies have shown that techniques of infrared spectroscopy have molecular sensitivity comparable to that of immunohistochemistry (IHC) in detecting biochemical changes in biological samples, and require less material, less effort, and are faster and cheaper.[16] Infrared spectroscopy can be used to detect the particle size distribution of microplastics in tissues, biofluids and living environments, and to understand the risk levels of these exposures to humans.[17] At present, ATR-FTIR spectroscopy has been widely used to understand changes in cells and tissues, especially those changes caused by exposure to environmental disrupting chemicals (EDCs), due to its ability to identify specific chemical changes in biological samples.[18] ATR-FTIR spectroscopy has been widely used in environmental toxicology studies, mainly for identifying the toxic effects of pollutants and exploring the mechanisms of toxic effects.[19] Zhu et al. assessed the toxicity of Cadmium (Cd) and mono-(2-ethylhexyl) phthalate (MEHP) using ATR-FTIR spectroscopy, and suggested that disruption of the cell membrane structure and integrity could be the common mechanism of Cd and MEHP toxicity in the liver, kidney, spleen, and lung.[20] In addition, ATR-FTIR spectroscopy can be used to identify biochemical differences in different cells, evaluate the susceptibility of different cell types to environmental pollutants, and thus influence the choice of cell types used in toxicology experiments.[19]

PBDEs and PAHs are persistent organic pollutants, which have become important due to their continuous accumulation in the environment and wildlife.[21] EDCs are exogenous substances that interfere with the synthesis of TH, the function of deiodinase in peripheral tissues, and the activation or antagonism of blood proteins and some chemicals to targeted receptors,[22] and B[*a*]P and BDE-47 are common EDCs. Some studies suggested that B[*a*]P could affect TH synthesis by inhibiting thyroid peroxidase (TPO) activity,[23] while BDE-47 does not alter the activity of TPO.[24] Other studies showed that the combined exposure of B[*a*]P and BDE-47 showed antagonism, that was, BDE-47 could significantly reduce the toxic effects induced by B[*a*]P.[25,26] In this study, oral exposure to B[*a*]P and BDE-47 in female Sprague−Dawley (SD) rats was modeled by evaluating ATR-FTIR spectroscopy to characterize the thyroid tissue effect of exposure to a single contaminant B[*a*]P and PBDEs homologous. The aim was also to determine whether the effects of contaminants could be predicted by the spectrochemical signature produced from the thyroid tissue treated with a single chemical component.

2. MATERIALS AND METHODS

2.1. Animals and Reagents. Twenty-four specific-pathogen free (SPF) adult female Sprague−Dawley (SD) rats (130 ± 10 g mean body weight) were bought from Hunan Slack Jingda Experimental Animal Co., Ltd. To explore the effects of B[*a*]P and BDE-47, all rats were housed in an SPF animal laboratory with a temperature of 21 ± 1 °C and a humidity of 50 ± 5%. The rats were exposed to light and dark conditions for 12 h each, with no restrictions on drinking water or diet. B[*a*]P was bought from Sigma (USA), with a purity of greater than 96%. BDE-47 was obtained from Toronto Research Chemicals (Canada) with a purity of greater than 99%. Corn oil was purchased from Acros Organics (Belgium).

2.2. Animal Treatment and Sample Collection. *2.2.1. Animal Exposure.* First, rats were adapted to the experimental conditions for 7 days. The rats were then randomly divided into three experimental groups, control (corn oil), B[*a*]P (5 mg/kg), and BDE-47 (0.5 mg/kg). The rats in each group were exposed to the substance by gavage once a day for 30 days. The rats were sacrificed 24 h after the last exposure and the thyroid gland was taken.

2.2.2. Histopathological Examination. After the rats were sacrificed, the thyroid gland was quickly removed, washed with precooling phosphate buffered saline, and their color and morphological changes were observed. After being fixed in 4% paraformaldehyde, the tissues were embedded in paraffin, and cut into 3 μm sections. The tissues were stained with Hematoxylin and eosin (H&E), and observed under a light microscope (magnifications 100× and 400×).

2.2.3. ATR-FTIR Spectroscopy. The remaining samples were permeated with optimal cutting temperature (OCT) embedding medium and then cryosectioned (8 μm thickness) perpendicular to the articular surface. Finally, the samples were air-dried. A few drops of ultrapure water were added to remove the OCT from the tissue section by pipetting off and then drying the section again. Afterward, the samples were floated on IR-reflective low-E slides (Kevley Technologies, Chesterland, OH, USA), and allowed to air-dry prior to spectral acquisition. The sample spectra were recorded from 32 randomly selected locations on each slide using a Bruker TENSOR 27 FTIR spectrometer equipped with a Helios ATR attachment containing a diamond crystal (Bruker Optics Ltd., UK). Measurements were made using 64 reading scans and 16 cm^{-1} spectral resolution. Before the next slide was measured, the ATR crystal was cleansed with deionized water, and a new background spectrum was measured before every new sample. The acquired spectra were converted into absorbance using the Bruker OPUS software and exported in.txt format files for further data processing in MATLAB R2014b (The MathWorks, Inc., USA).

The acquired spectral data were processed using PLS Toolbox 7.9.3 (eigenvector Research, Inc., USA) running on MATLAB R2014b. For this, the spectra were initially truncated to the biofingerprint region (900−1800 cm^{-1}) to reduce atmospheric interferences existing in other spectral regions. Thereafter, the Savitzky−Golay second derivative (7 points window, second order polynomial fitting) and vector normalization were applied to correct the spectral baseline and to enhance differences between the spectral features. Subsequently, the sample spectra were split into training (70%) and test (30%) sets using the Kennard-Stone algorithm. For this, the training group is selected from the whole set of samples based on a Euclidian distance calculation performed by assigning the sample with the maximum distance from all other samples to the training set, and then, by choosing the samples that are as far away as possible from the initially selected sample to this same set, until the desired number of samples is finally obtained in the training set.[27] The samples not chosen for the training set are therefore assigned for the test set. The training set is used for model construction, while the test set is used for model validation. Support vector machine (SVM)[28] was used for spectral discrimination. SVM is a binary linear classifier with a nonlinear step called the kernel transformation, which transforms the input spectral data space

https://doi.org/10.1021/acsomega.3c05819
ACS Omega 2024, 9, 4317−4323

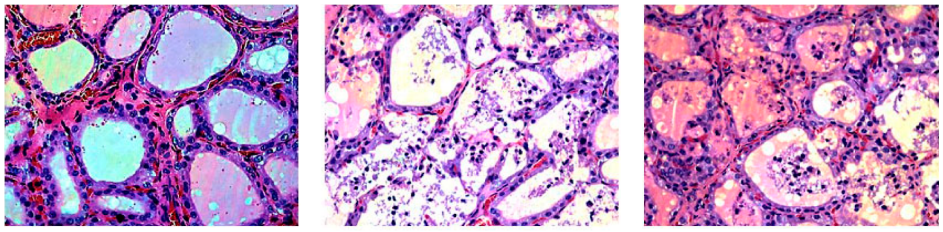

Figure 1. Pathological results of control and exposed thyroid samples under a light microscope (×400). (a) Solvent control group (corn oil); (b) 5 mg/kg B[*a*]P treatment group; and (c) 0.5 mg/kg BDE-47 treatment group.

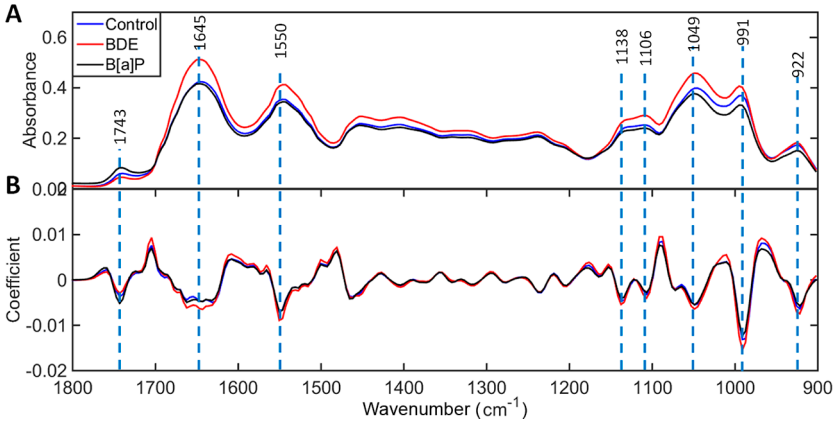

Figure 2. Infrared (IR) spectra for controls (blue), 2,20,4,40-tetrabromodiphenyl ether (BDE-47)-treated (red) and benzo[*a*]pyrene (B[*a*]P)-treated (black) before and after preprocessing. (A) Mean raw spectra in the biofingerprint region (1800−900 cm^{-1}) for control, BDE, and B[*a*]P groups; (B) Mean preprocessed spectra [Savitzky−Golay 2nd derivative (window of 7 points, 2nd order polynomial fitting) followed by vector normalization] in the biofingerprint region (1800−900 cm^{-1}) for controls, BDE, and B[*a*]P groups. The wavenumbers for the main spectral features are inserted.

into a nonlinear feature space that maximizes the spectra separation between known groups. Then, a linear discrimination is performed between the spectra of this feature space. SVM was run using a radial-basis function kernel and optimized with cross-validation venetian blinds (10 data splits). Figures of merit, including accuracy, sensitivity, and specificity, were then calculated for the external test set used for model validation.

3. RESULTS

3.1. Pathological Changes of Rat Thyroid Tissue after Hematoxylin and Eosin Staining. Under the microscope, the follicles in the control group were round or oval in different sizes with a clear boundary. The cavity of the follicles was filled with a homogeneous colloid, and there were vacuoles. The parafollicular cells were located between the thyroid follicles and epithelial cells. The cells were slightly larger and had a single-layered cubic shape, with lighter cytoplasmic coloration and a round nucleus (Figure 1a).

The morphology of rat thyroid cells treated with 5 mg/kg of B[*a*]P and 0.5 mg/kg of BDE-47 changed. Microscopically, in the B[*a*]P group, it was found that a part of the thyroid follicle structure was destroyed, the follicular epithelial cells were necrotic and shed into the follicular cavity, the glial cells accumulated in the individual follicular cavity, and the color was darker (Figure 1b). In the BDE-47 treatment group, the follicle structure was deformed in the middle and marginal parts of the gland, and the follicles were flat or low columnar. Parts of the follicular epithelial cells were necrotic and fell into the follicular cavity, and the follicular space became larger; some of the follicles with colloids gathered in the middle were darker (Figure 1c).

3.2. Changes of Thyroid in ATR-FTIR. From the 24 samples, 768 spectra (i.e., 32 spectra per sample) were obtained. Figure 2 shows the effect of the spectral data before (Figure 2a) and after (Figure 2b) preprocessing (biofingerprint region, Savitzky−Golay second derivative [window of 7 points, second order polynomial fitting] and vector normalization). Differences in the main spectral features at 1800 to 900 cm^{-1} were observed between the control group and all treatment groups.

The spectral classification into control and treatment groups was performed using SVM (Tables 1 and 2). First, the

Table 1. Classification Performance for Control vs (BPDE, B[*a*]P) Samples Using a SVM

subset	accuracy (%)	sensitivity (%)	specificity (%)
training	100	100	100
cross-validation	92	95	75
Test	96	98	87

Table 2. Classification Performance for BDE vs B[*a*]P Samples Using SVM

subset	accuracy (%)	sensitivity (%)	specificity (%)
training	100	100	100
cross-validation	86	88	84
test	93	94	92

https://doi.org/10.1021/acsomega.3c05819
ACS Omega 2024, 9, 4317−4323

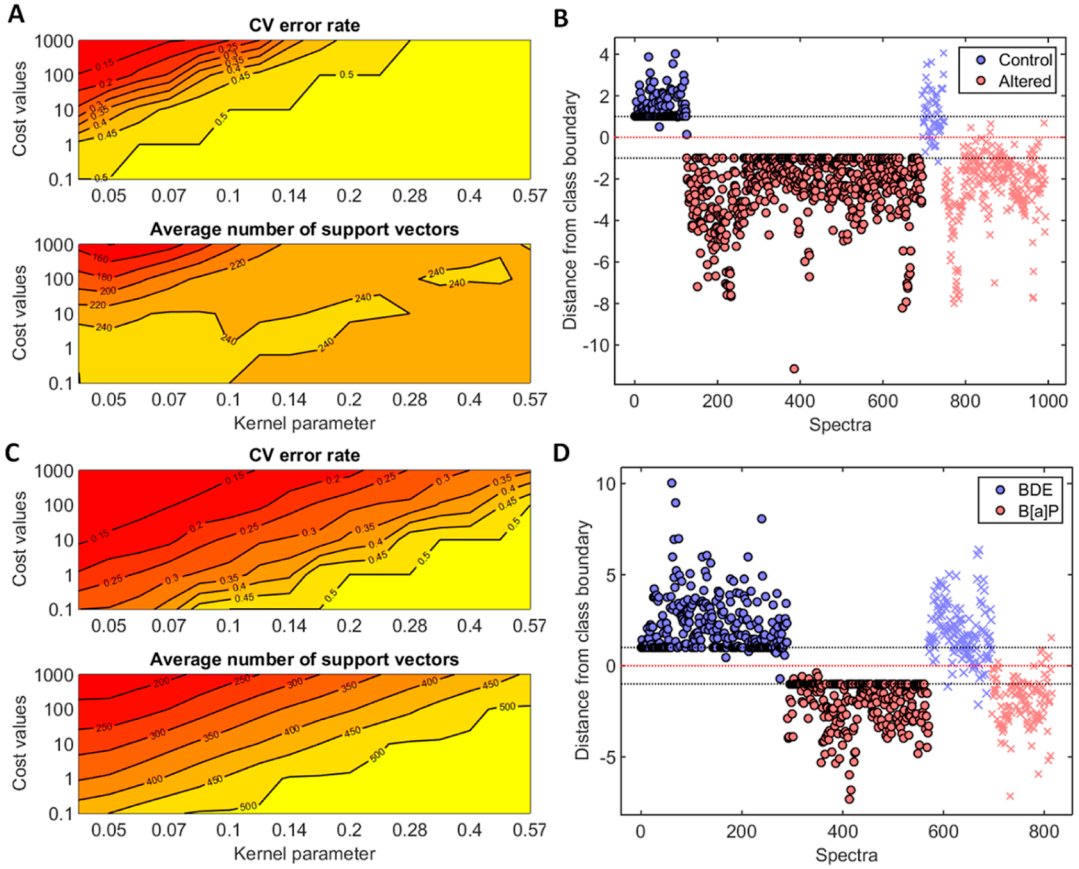

Figure 3. SVM results to discriminate controls vs treatment samples, and for BDE-47 (2,20,4,40-tetrabromodiphenyl ether) vs benzo[*a*]pyrene (B[*a*]P). (A) SVM cross-validation (CV) optimization to distinguish controls vs altered (BDE-47 and B[*a*]P); (B) SVM discriminant graph for controls vs altered (BDE-47 and B[*a*]P); (C) SVM cross-validation (CV) optimization to distinguish BDE-47 vs B[*a*]P; and (D) SVM discriminant graph for BDE-47 vs B[*a*]P. Spectra: training (o), test (x).

treatment group (altered group) were compared with the control group, and then, the comparison between two exposure groups was carried out. As observed, when the classification was performed using SVM, there is a substantial separation between the samples from control and altered classes (accuracy = 96%; sensitivity = 98%; specificity = 87%). Likewise, there is a major separation between the exposed groups (accuracy = 93%; sensitivity = 94%; specificity = 92%), indicating these two groups are quite distinct from the others. The cost function for SVM optimization during cross-validation and SVM discriminant graphs in terms of predicted probability for controls versus altered class, and for BPDE versus B[*a*]P are shown in Figure 3.

Since specific wavenumbers in the infrared spectra can be used as a biomarker of chemical structures in tissues or cells, their absorption intensity can be used to evaluate the biological effects of pollutants exposed to the tissues after preprocessing. The main features for the control, the BDE-47 and the B[*a*]P groups were related to C═O stretch vibrations of lipids (1743 cm^{-1}), as well as the secondary structure of proteins [amide I (1645 cm^{-1}) and amide II (1550 cm^{-1})], and carbohydrates [C−OH (1138 cm^{-1}), C−O (1106 cm^{-1}, 1049 cm^{-1}, 991 cm^{-1}), C−C (1106 cm^{-1}) stretching], and collagen (phosphodiester stretching at 922 cm^{-1}) vibration modes (Table 3).

Table 3. Main Spectral Features for Controls, BDE-47, and B[*a*]P[a]

spectral feature (cm^{-1})	tentative assignment	*P*-value
1743	C═O stretching (lipids)	10^{-6} (**)
1645	amide I (proteins)	10^{-9} (**)
1550	amide II (proteins)	10^{-10} (**)
1138	C−OH stretching (oligosaccharides)	10^{-13} (**)
1106	C−O, C−C stretching (polysaccharides, pectin)	10^{-25} (**)
1049	C−O stretching coupled with C−O bending (carbohydrates)	0.002 (*)
991	C−O stretching (ribose)	10^{-9} (**)
922	phosphodiester stretching (collagen, glycogen)	10^{-17} (**)

[a]*P*-Values calculated based on an ANOVA test between the three groups (controls, BDE-47, and B[*a*]P). $P < 0.05$ was considered statistically significant (*), and $P < 0.001$ was considered statistically highly significant (**).

4. DISCUSSION

In recent years, some studies have demonstrated that EDCs (including B[*a*]P and BDE-47) affect thyroid structure and hormone secretion.[11,29] Here, we employed ATR-FTIR

https://doi.org/10.1021/acsomega.3c05819
ACS Omega 2024, 9, 4317−4323

spectroscopy coupled with SVM to probe the changes of thyroid tissue and biochemical structure after exposure of B[*a*]P and BDE-47 to rats. This study showed that after B[*a*]P and BDE-47 treatment, the structure of thyroid follicles of rats was destroyed and epithelial cells were necrotic, indicating that B[*a*]P and BDE-47 may lead to changes of thyroid morphology and/or pathological. Previous studies in rats and fish had similar findings. The thyroid tissue structure and secretion changed significantly after *Liza Abu* was exposed to B[*a*]P for 2 weeks.[29] B[*a*]P exposure significantly decreased the circulatory concentrations of T3 and T4 and increased the circulatory concentrations of thyroid-stimulating hormone in the treated rats and fish.[29,30] Another study suggested that the primary toxic effects of short-term exposure to B[*a*]P in zebrafish was compromised hypothalamic-pituitary function, which would then hamper the adequate functional maturation of thyroid follicles and TH synthesis. The main toxic effect of short-term exposure to B[*a*]P in zebrafish is impaired hypothalamic-pituitary function, which prevents the full functional maturation of thyroid follicles and hormone synthesis.[31] BDE-47 exposure in vivo can alter the secretion of thyroid hormones and change the status of thyroid gland in rats and fish.[9−11] Elevated serum T3 levels after exposure to BDE-47 in rats are consistent with an epidemiological study showing that plasma concentrations of BDE-47 in adults are positively correlated with serum T3 levels.[32,33] A systematic review suggests that exposure to PBDEs and the interaction of PBDEs (or their metabolites) with the TH transport system or thyroid receptors may lead to increased T4 metabolism and excretion.[34] Interestingly, the effects of B[*a*]P and BDE-47 on thyroid metabolism may be antagonistic, which must be confirmed by further studies. Studies have suggested that the possible mechanism of thyroid disruption induced by BDE-47 is as follows: BDE-47 is a powerful human pregnane X receptor (hPXR) activator, and the activation of hPXR plays an important role in the down-regulation of BDE-47 induced thyroid receptor, and the up-regulation of CYP3A4, UGT1A3 and SULT2A1 are involved in this process.[35] However, the exact mechanisms of thyroid injury caused by B[*a*]P are still elusive.

ATR-FTIR is a technology which can be used to detect the different biological effects of target cells caused by chemical pollutants,[36] which has played a significant role in the study of cancer and the assessment of the effects of toxic effects on environmental pollution.[37] Benign and malignant tumors in tissue samples can be distinguished by the use of infrared spectroscopy as an imaging tool or by classification of spectral categories.[38] Herein, we found that the spectral range of 1800−900 cm^{-1} has the most significant difference in the visible spectrum between the control class and the exposure class. Our results showed that the distinguishing wavenumbers induced by B[*a*]P and BDE-47 treatments were mainly associated with lipids, protein amides (amide I and amide II), carbohydrate and collagen vibration modes, similar to previous reported research results.[39] Lipids, carbohydrates, and collagen are related to the outer membrane of cells, while proteins are the main executors to efficiently modify the biological activity of cells. The modifications of these intracellular macromolecules are key molecular events in response to environmental perturbation. Our findings suggest that B[*a*]P and BDE-47 exposure generated a range of biomolecular alterations associated with structural proteins and lipids/carbohydrates. Possibly, B[*a*]P and BDE-47 alter essential constituents of cell membranes, leading to cell injury, which, in turn, destroys cellular biomolecules. The amide I and amide II bands are the most sensitive probes for monitoring conformational changes of the secondary structure of proteins.[40] In our study, the characteristic bands for Amide I and Amide II are clearly observed, indicating abnormal protein structure and impaired cell function caused by B[*a*]P and BDE-47 exposure.[41]

In order to maximize the accuracy, sensitivity, and specificity of ATR-FTIR spectroscopy, the spectral data must be preprocessed to ensure that important biological information will not be concealed or diluted by noise or systematic variation,[42] and then, the preprocessed data undergo multivariate analysis or machine learning techniques for spectral discrimination. Figure 3 shows that SVM can use the spectral data generated by ATR-FTIR spectroscopy to clearly classify and predict the subsequent thyroid gland of rats after exposure to B[*a*]P and BDE-47. In this study, discrimination between control versus altered (BPDE, B[*a*]P) groups were found at 96% accuracy, and between BPDE versus B[*a*]P at 93% accuracy, indicating the feasibility of ATR-FTIR to detect biochemical changes in the analyzed samples. However, further research is needed to assess the risk of individual *versus* binary mixture exposures to B[*a*]P and BDE-47.

5. CONCLUSIONS

Both B[*a*]P and BDE-47 may cause damage to the rat's thyroid. In this study, the absorption intensity of different functional groups in the control and exposure (B[*a*]P, BDE-47) groups were evaluated using ATR-FTIR spectroscopy and classified by SVM. The results demonstrate that long-term exposure to B[*a*]P and BDE-47 could affect the molecular structure and function of lipid metabolism, protein secondary structure, carbohydrate, and ribose in rat thyroid. Future studies are needed to explore the mechanisms of how the exposure of B[*a*]P and BDE-47 affect thyroid function and hormone.

AUTHOR INFORMATION

Corresponding Authors

Camilo L. M. Morais − *Center for Education, Science and Technology of the Inhamuns Region, State University of Ceará, Tauá 63660-000, Brazil*; Email: camilo.morais@uece.br

Hui Liu − *Guangxi Key Laboratory of Environmental Exposomics and Entire Lifecycle Heath, Guilin Medical University, Guilin, Guangxi 541199, China; School of Public Health, Guilin Medical University, Guilin, Guangxi 541199, China*; Email: huihuiabcd@126.com

Authors

QiuFeng Lao − *Guangxi Key Laboratory of Environmental Exposomics and Entire Lifecycle Heath, Guilin Medical University, Guilin, Guangxi 541199, China; School of Public Health, Guilin Medical University, Guilin, Guangxi 541199, China; Liuzhou People's Hospital, Liuzhou, Guangxi 545006, China;* orcid.org/0000-0001-5562-4687

LiJun Yang − *Guangxi Key Laboratory of Environmental Exposomics and Entire Lifecycle Heath, Guilin Medical University, Guilin, Guangxi 541199, China; School of Public Health, Guilin Medical University, Guilin, Guangxi 541199, China*

https://doi.org/10.1021/acsomega.3c05819
ACS Omega 2024, 9, 4317−4323

ShuZhen Liu − *Guangxi Key Laboratory of Environmental Exposomics and Entire Lifecycle Heath, Guilin Medical University, Guilin, Guangxi 541199, China; School of Public Health, Guilin Medical University, Guilin, Guangxi 541199, China*

XiaoJun Ma − *Guangxi Key Laboratory of Environmental Exposomics and Entire Lifecycle Heath, Guilin Medical University, Guilin, Guangxi 541199, China; School of Public Health, Guilin Medical University, Guilin, Guangxi 541199, China*

DeChan Tan − *Guangxi Key Laboratory of Environmental Exposomics and Entire Lifecycle Heath, Guilin Medical University, Guilin, Guangxi 541199, China; School of Public Health, Guilin Medical University, Guilin, Guangxi 541199, China*

JinBo Li − *Guangxi Key Laboratory of Environmental Exposomics and Entire Lifecycle Heath, Guilin Medical University, Guilin, Guangxi 541199, China; School of Public Health, Guilin Medical University, Guilin, Guangxi 541199, China*

BaoYi Liao − *Guangxi Key Laboratory of Environmental Exposomics and Entire Lifecycle Heath, Guilin Medical University, Guilin, Guangxi 541199, China; School of Public Health, Guilin Medical University, Guilin, Guangxi 541199, China*

YuanFeng Wei − *Guangxi Key Laboratory of Environmental Exposomics and Entire Lifecycle Heath, Guilin Medical University, Guilin, Guangxi 541199, China; School of Public Health, Guilin Medical University, Guilin, Guangxi 541199, China*

WeiYi Pang − *Guangxi Key Laboratory of Environmental Exposomics and Entire Lifecycle Heath, Guilin Medical University, Guilin, Guangxi 541199, China*

Complete contact information is available at: https://pubs.acs.org/10.1021/acsomega.3c05819

Author Contributions

⊥joint-first authors.

Notes

The authors declare no competing financial interest.

■ ACKNOWLEDGMENTS

The study was supported by Guangxi Science and Technology Base and Talent Special Project (grant number AD18050005).

■ REFERENCES

(1) Ravindra, K.; Sokhi, R.; Vangrieken, R. Atmospheric polycyclic aromatic hydrocarbons: Source attribution, emission factors and regulation. *Atmos. Environ.* **2008**, *42* (13), 2895−2921.

(2) Kim, K. H.; Jahan, S. A.; Kabir, E.; Brown, R. J. A review of airborne polycyclic aromatic hydrocarbons (PAHs) and their human health effects. *Environ. Int.* **2013**, *60*, 71−80.

(3) Boas, M.; Feldt-Rasmussen, U.; Skakkebaek, N. E.; Main, K. M. Environmental chemicals and thyroid function. *Eur. J. Endocrinol.* **2006**, *154* (5), 599−611.

(4) Boström, C.-E.; Gerde, P.; Hanberg, A.; Jernström, B.; Johansson, C.; Kyrklund, T.; Rannug, A.; Törnqvist, M.; Victorin, K.; Westerholm, R. Cancer risk assessment, indicators, and guidelines for polycyclic aromatic hydrocarbons in the ambient air. *Environ. Health Perspect.* **2002**, 451−488.

(5) Phillips, D. Fifty years of benzo(a)pyrene. *Nature* **1983**, *303* (5917), 468−472.

(6) Li, C. Y.; Dempsey, J. L.; Wang, D.; Lee, S.; Weigel, K. M.; Fei, Q.; Bhatt, D. K.; Prasad, B.; Raftery, D.; Gu, H.; Cui, J. Y. PBDEs Altered Gut Microbiome and Bile Acid Homeostasis in Male C57BL/6 Mice. *Drug Metab. Dispos.* **2018**, *46* (8), 1226−1240.

(7) Frederiksen, M.; Vorkamp, K.; Thomsen, M.; Knudsen, L. E. Human internal and external exposure to PBDEs-a review of levels and sources. *Int. J. Hyg Environ. Health* **2009**, *212* (2), 109−134.

(8) Erratico, C. A.; Moffatt, S. C.; Bandiera, S. M. Comparative oxidative metabolism of BDE-47 and BDE-99 by rat hepatic microsomes. *Toxicol. Sci.* **2011**, *123* (1), 37−47.

(9) Lema, S. C.; Dickey, J. T.; Schultz, I. R.; Swanson, P. Dietary exposure to 2,2',4,4'-tetrabromodiphenyl ether (PBDE-47) alters thyroid status and thyroid hormone-regulated gene transcription in the pituitary and brain. *Environ. Health Perspect.* **2008**, *116* (12), 1694−1699.

(10) Skarman, E.; Darnerud, P. O.; Ohrvik, H.; Oskarsson, A. Reduced thyroxine levels in mice perinatally exposed to polybrominated diphenyl ethers. *Environ. Toxicol. Pharmacol.* **2005**, *19* (2), 273−281.

(11) Talsness, C. E.; Kuriyama, S. N.; Sterner-Kock, A.; Schnitker, P.; Grande, S. W.; Shakibaei, M.; Andrade, A.; Grote, K.; Chahoud, I. In utero and lactational exposures to low doses of polybrominated diphenyl ether-47 alter the reproductive system and thyroid gland of female rat offspring. *Environ. Health Perspect.* **2008**, *116* (3), 308−314.

(12) Xu, P.; Lou, X.; Ding, G.; Shen, H.; Wu, L.; Chen, Z.; Han, J.; Wang, X. Effects of PCBs and PBDEs on thyroid hormone, lymphocyte proliferation, hematology and kidney injury markers in residents of an e-waste dismantling area in Zhejiang, China. *Sci. Total Environ.* **2015**, *536*, 215−222.

(13) Huang, F.; Wen, S.; Li, J.; Zhong, Y.; Zhao, Y.; Wu, Y. The human body burden of polybrominated diphenyl ethers and their relationships with thyroid hormones in the general population in Northern China. *Sci. Total Environ.* **2014**, *466−467*, 609−615.

(14) Martin, F. L.; Kelly, J. G.; Llabjani, V.; Martin-Hirsch, P. L.; Patel, I. I.; Trevisan, J.; Fullwood, N. J.; Walsh, M. J. Distinguishing cell types or populations based on the computational analysis of their infrared spectra. *Nat. Protoc.* **2010**, *5* (11), 1748−1760.

(15) Raab, S. S.; Grzybicki, D. M. Quality in cancer diagnosis. *Ca - Cancer J. Clin.* **2010**, *60* (3), 139−165.

(16) Diem, M.; Ergin, A.; Remiszewski, S.; Mu, X.; Akalin, A.; Raz, D. Infrared micro-spectroscopy of human tissue: principles and future promises. *Faraday Discuss.* **2016**, *187*, 9−42.

(17) Wright, S.; Levermore, J.; Ishikawa, Y. Application of Infrared and Near-Infrared Microspectroscopy to Microplastic Human Exposure Measurements. *Appl. Spectrosc.* **2023**, *77* (10), 1105−1128.

(18) Wang, L.; Mizaikoff, B. Application of multivariate data-analysis techniques to biomedical diagnostics based on mid-infrared spectroscopy. *Anal. Bioanal. Chem.* **2008**, *391* (5), 1641−1654.

(19) Heys, K.; Shore, R.; Pereira, M.; Martin, F. Vibrational biospectroscopy characterizes biochemical differences between cell types used for toxicological investigations and identifies alterations induced by environmental contaminants. *Environ. Toxicol. Chem.* **2017**, *36* (11), 3127−3137.

(20) Zhu, L.; Duan, P.; Hu, X.; Wang, Y.; Chen, C.; Wan, J.; Dai, M.; Liang, X.; Li, J.; Tan, Y. Exposure to cadmium and mono-(2-ethylhexyl) phthalate induce biochemical changes in rat liver, spleen, lung and kidney as determined by attenuated total reflection-Fourier transform infrared spectroscopy. *J. Appl. Toxicol.* **2019**, *39* (5), 783−797.

(21) An, J.; Yin, L.; Shang, Y.; Zhong, Y.; Zhang, X.; Wu, M.; Yu, Z.; Sheng, G.; Fu, J.; Huang, Y. The combined effects of BDE47 and BaP on oxidatively generated DNA damage in L02 cells and the possible molecular mechanism. *Mutat. Res.* **2011**, *721* (2), 192−198.

(22) Brar, N. K.; Waggoner, C.; Reyes, J. A.; Fairey, R.; Kelley, K. M. Evidence for thyroid endocrine disruption in wild fish in San Francisco Bay, California, USA. Relationships to contaminant exposures. *Aquat. Toxicol.* **2010**, *96* (3), 203−215.

(23) Song, M.; Kim, Y. J.; Park, Y. K.; Ryu, J. C. Changes in thyroid peroxidase activity in response to various chemicals. *J. Environ. Monit* **2012**, *14* (8), 2121−2126.

(24) Wu, Y.; Beland, F. A.; Fang, J. L. Effect of triclosan, triclocarban, 2,2',4,4'-tetrabromodiphenyl ether, and bisphenol A on the iodide uptake, thyroid peroxidase activity, and expression of genes involved in thyroid hormone synthesis. *In Vitro Toxicol.* **2016**, *32*, 310−319.
(25) Zhao, Y.; Luo, K.; Fan, Z.; Huang, C.; Hu, J. Modulation of benzo[a]pyrene-induced toxic effects in Japanese medaka (Oryzias latipes) by 2,2',4,4'-tetrabromodiphenyl ether. *Environ. Sci. Technol.* **2013**, *47* (22), 13068−13076.
(26) Xie, J.; Yang, D.; Sun, X.; Cao, R.; Chen, L.; Wang, Q.; Li, F.; Wu, H.; Ji, C.; Cong, M.; Zhao, J. Individual and Combined Toxicities of Benzo[a]pyrene and 2,2',4,4'-Tetrabromodiphenyl Ether on Early Life Stages of the Pacific Oyster, Crassostrea gigas. *Bull. Environ. Contam. Toxicol.* **2017**, *99* (5), 582−588.
(27) Morais, C.; Lima, K.; Singh, M.; Martin, F. Tutorial: multivariate classification for vibrational spectroscopy in biological samples. *Nat. Protoc.* **2020**, *15* (7), 2143−2162.
(28) Cortes, C.; Vapnik, V. Support-Vector Networks. *Mach. Learn.* **1995**, *20*, 273−297.
(29) Movahedinia, A.; Salamat, N.; Kheradmand, P. Effects of the environmental endocrine disrupting compound benzo[a]pyrene on thyroidal status of abu mullet (Liza abu) during short-term exposure. *Toxicol Rep* **2018**, *5*, 377−382.
(30) Adedara, I. A.; Daramola, Y. M.; Dagunduro, J. O.; Aiyegbusi, M. A.; Farombi, E. O. Renoprotection of Kolaviron against benzo (A) pyrene-induced renal toxicity in rats. *Ren. Fail.* **2015**, *37* (3), 497−504.
(31) Rurale, G.; Gentile, I.; Carbonero, C.; Persani, L.; Marelli, F. Short-Term Exposure Effects of the Environmental Endocrine Disruptor Benzo(a)Pyrene on Thyroid Axis Function in Zebrafish. *Int. J. Mol. Sci.* **2022**, *23* (10), 5833.
(32) Li, X.; Gao, H.; Li, P.; Chen, W.; Tang, S.; Liu, L.; Zhou, G.; Xia, T.; Wang, A.; Zhang, S. Impaired sperm quantity and motility in adult rats following gestational and lactational exposure to environmentally relevant levels of PBDE-47: A potential role of thyroid hormones disruption. *Environ. Pollut.* **2021**, *268*, 115773.
(33) Dallaire, R.; Dewailly, E.; Pereg, D.; Dery, S.; Ayotte, P. Thyroid function and plasma concentrations of polyhalogenated compounds in Inuit adults. *Environ. Health Perspect.* **2009**, *117* (9), 1380−1386.
(34) Costa, L. G.; de Laat, R.; Tagliaferri, S.; Pellacani, C. A mechanistic view of polybrominated diphenyl ether (PBDE) developmental neurotoxicity. *Toxicol. Lett.* **2014**, *230* (2), 282−294.
(35) Hu, X.; Zhang, J.; Jiang, Y.; Lei, Y.; Lu, L.; Zhou, J.; Huang, H.; Fang, D.; Tao, G. Effect on metabolic enzymes and thyroid receptors induced by BDE-47 by activation the pregnane X receptor in HepG2, a human hepatoma cell line. *In Vitro Toxicol.* **2014**, *28* (8), 1377−1385.
(36) Llabjani, V.; Trevisan, J.; Jones, K. C.; Shore, R. F.; Martin, F. L. Binary mixture effects by PBDE congeners (47, 153, 183, or 209) and PCB congeners (126 or 153) in MCF-7 cells: biochemical alterations assessed by IR spectroscopy and multivariate analysis. *Environ. Sci. Technol.* **2010**, *44* (10), 3992−3998.
(37) Li, J.; Tian, M.; Cui, L.; Dwyer, J.; Fullwood, N. J.; Shen, H.; Martin, F. L. Low-dose carbon-based nanoparticle-induced effects in A549 lung cells determined by biospectroscopy are associated with increases in genomic methylation. *Sci. Rep.* **2016**, *6*, 20207.
(38) Baker, M. J.; Trevisan, J.; Bassan, P.; Bhargava, R.; Butler, H. J.; Dorling, K. M.; Fielden, P. R.; Fogarty, S. W.; Fullwood, N. J.; Heys, K. A.; Hughes, C.; Lasch, P.; Martin-Hirsch, P. L.; Obinaju, B.; Sockalingum, G. D.; Sule-Suso, J.; Strong, R. J.; Walsh, M. J.; Wood, B. R.; Gardner, P.; Martin, F. L. Using Fourier transform IR spectroscopy to analyze biological materials. *Nat. Protoc.* **2014**, *9* (8), 1771−1791.
(39) Llabjani, V.; Trevisan, J.; Jones, K.; Shore, R.; Martin, F. Binary mixture effects by PBDE congeners (47, 153, 183, or 209) and PCB congeners (126 or 153) in MCF-7 cells: biochemical alterations assessed by IR spectroscopy and multivariate analysis. *Environ. Sci. Technol.* **2010**, *44* (10), 3992−3998.
(40) Duan, P.; Liu, B.; Morais, C.; Zhao, J.; Li, X.; Tu, J.; Yang, W.; Chen, C.; Long, M.; Feng, X.; Martin, F.; Xiong, C. 4-Nonylphenol effects on rat testis and sertoli cells determined by spectrochemical techniques coupled with chemometric analysis. *Chemosphere* **2019**, *218*, 64−75.
(41) Liu, G.; Sheng, H.; Fu, Y.; Song, Y.; Redmile-Gordon, M.; Qiao, Y.; Gu, C.; Xiang, L.; Wang, F. Extracellular polymeric substances (EPS) modulate adsorption isotherms between biochar and 2,2',4,4'-tetrabromodiphenyl ether. *Chemosphere* **2019**, *214*, 176−183.
(42) Butler, H. J.; Smith, B. R.; Fritzsch, R.; Radhakrishnan, P.; Palmer, D. S.; Baker, M. J. Optimised spectral pre-processing for discrimination of biofluids via ATR-FTIR spectroscopy. *Analyst* **2018**, *143* (24), 6121−6134.

https://doi.org/10.1021/acsomega.3c05819
ACS Omega 2024, 9, 4317−4323